IEEE Access
Multidisciplinary | Rapid Review | Open Access Journal

Received July 12, 2018, accepted August 17, 2018, date of publication August 21, 2018, date of current version September 7, 2018.

*Digital Object Identifier 10.1109/ACCESS.2018.2866479*

# Rotational Speed Measurement Through Image Similarity Evaluation and Spectral Analysis

**TIANYU WANG[1], (Member, IEEE), YONG YAN[2], (Fellow, IEEE), LIJUAN WANG[2], (Member, IEEE), AND YONGHUI HU[1], (Member, IEEE)**

[1]School of Control and Computer Engineering, North China Electric Power University, Beijing 102206, China
[2]School of Engineering and Digital Arts, University of Kent, Canterbury CT2 7NT, U.K.

Corresponding author: Yong Yan (y.yan@kent.ac.uk)

This work was supported in part by the National Natural Science Foundation of China under Grant 51375163 and in part by the Fundamental Research Funds for the Central Universities under Grant 2017XS157.

**ABSTRACT** Accurate and reliable measurement of rotational speed is desirable in a variety of industries. This paper presents a rotational speed measurement system based on a low-cost imaging device with a simple marker on the rotor. Sequential images are pre-processed through denoising, histogram equalization, and circle Hough transform, and then processed by similarity evaluation methods to obtain the similarity level of images. Finally, the rotational speed is obtained through the Chirp-Z transform on the restructured signals. The measurement principle, structure design, and performance assessment of the proposed system are presented. The effects of different influence factors, including frame rate, marker shape and size, an algorithm for image similarity evaluation, illumination conditions, shooting angle and photographic distance, on the performance of the measurement system are quantified and discussed through a series of experimental tests on a laboratory test rig. Experimental results suggest that the system is capable of providing constant rotational speed measurement with a maximum relative error of $\pm 0.6\%$ and a repeatability of less than 0.6% over a speed range from 100 to 900 RPM. Under varying speed conditions the proposed system can achieve valid measurement with a relative error within $\pm 1\%$ over the speed range of 300 to 900 RPM.

**INDEX TERMS** Image processing, rotational speed measurement, spectral analysis, tachometer.

## I. INTRODUCTION

Rotating machineries such as generators, electromotors and centrifuges play an important role in a wide range of industries. As one of the crucial parameters for rotating machineries, rotational speed is essential for system condition monitoring, process control and fault diagnosis. Consequently, online continuous measurement of rotational speed is required in a variety of industrial processes. Rotational speed metering devices can be divided into two types according to their measurement principles: contact and non-contact. A contact tachometer is normally mounted on the object being measured and hence suffers from wear problems particularly after a long period of usage. Moreover, the additional mass to the system may affect the dynamic characteristics of the rotor to be measured. A variety of non-contact tachometers based on optical, electrical, and magnetic induction principles have also been developed [1]–[3]. However, each technique has its individual limitations and cannot adapt to all industrial environments. For instance, the operation of a magnetic tachometer requires a ferromagnet to be installed on the rotor and the system performance is susceptible to electromagnetic interference. Photoelectric tachometers do not perform well under dusty, harsh and extreme conditions. Such instruments should be placed adjacent to the rotors being measured, which results in limited portability and flexibility in installation. Additionally, the delicate optical components of photoelectric tachometers may be contaminated by dust [4]. The electrostatic tachometers [5], [6] are little affected by environmental factors, but they are unsuitable for very low speed measurement due to insufficient electrostatic charge generated on the rotor surface. More recently, vibration signal processing techniques have been combined with accelerometers to estimate the rotational speed of rotating equipment [7]. However, such systems are difficult to obtain accurate measurements in a harsh industrial environment. When significant noise exists in the vibration signal, it will generate severe spectral interference and thus have an adverse effect on the rotational speed measurement [8].

Most existing tachometers have to be mounted on or placed adjacent to the rotors be measured and this has limited their

wide applicability due to cumbersome and costly installation and maintenance of sensors and data acquisition systems. For this reason conventional tachometers may not be suitable for applications under certain conditions due to the limitations of equipment assembly and on-site environments, for instance, the condition monitoring of large-scale mechanical systems under high-temperature or high-radiation environments such as gas turbines or wind turbines. In addition, convenient tachometers are point-wise sensors and provide only single channel speed data, which may not meet the requirements of certain industrial monitoring applications. To surmount these difficulties, significant efforts have been made to explore novel techniques that can advance the current state-of-the-art in rotational speed measurement. Due to the recent development of imaging sensors and image processing techniques, imaging based methods for rotational speed measurement offer a promising alternative to conventional techniques [9]–[14]. In comparison with conventional techniques for rotational speed measurement, the imaging based method has the advantages of remote measurement, simple installation, high robustness and wide applicability. The imaging device does not require physical access to the object to be measured and can be set up at a remote location even hundreds of meters away (when a zoom lens is used). Moreover, the imaging sensor can be regarded as a sensor array capable of simultaneously tracking multiple points and providing multi-channel speed data without extra hardware. Meanwhile, rich information in images has a great potential for determining other important parameters of a mechanical system such as vibration mode, allowing multi-source data fusion and thus achieving more efficient and systematic condition monitoring and fault diagnosis. High-speed cameras incorporating sophisticated imaging techniques have been applied to achieve rotational speed determination and rotational angle measurement. Guo *et al.* [10] proposed a template-based Lucus-Kanade algorithm to measure the rotational speed of a cylindrical coupling through tracking the rotating object in a video sequence. A rotational speed measurement system using a high-speed camera and a double-sine-varying-density fringe pattern was proposed by Zhong *et al*. [11]. However, imaging based rotational speed measurement is deceptively simple. The existing measurement systems based on imaging principle commonly use spatial domain methods that determine the ratio of the angular displacement of the rotating object to the time difference between two sequential frames. The displacement extraction is determined by pointwise searching the corresponding points between two sequential frames and has hence high computation complexity. In addition, the localization of the rotating object in the image may be adversely affected by motion blur. To ensure measurement accuracy, high-speed cameras are used in these approaches to obtain clear images by limiting exposure time to a lower value. It is claimed that the maximum measurable rotational speed using a high-speed camera with a frame rate of 800 fps (frames per second) is 960 RPM with a relative error less than 6% [10]. The low affordability of the high-speed camera limits the wide applicability of this technique, it is therefore desirable to develop techniques that use low-cost imaging sensors to achieve satisfactory rotational speed measurement.

This paper addresses the key issues systematically in low-cost imaging based measurement of rotational speed. The methodology incorporates dedicated algorithms for image similarity evaluation and frequency determination, transforming the problem of estimating the rotational speed into that of determining the main frequency of the image similarity signal, which has not been reported in the literature. The basic principle of rotational speed measurement using a low-cost imaging device along with some preliminary results was reported at the IEEE International Instrumentation and Measurement Technology Conference in 2017 [15]. However, the original measurement system did not perform well with limited sampling time due to the use of Fourier transform. Additionally, the effects of various key factors on the measurement system performance are not quantified. In the present paper novel algorithms and systematic experimental investigations with detailed data analysis are included. Firstly, algorithms for image pre-processing and Chirp-Z transform are deployed to enhance the measurement accuracy and resolution of the low-cost imaging system. Meanwhile, the effects of all key factors, including frame rate, marker shape and size, similarity evaluation algorithm, shooting angle, photographic distance and illumination conditions, on the performance of the measurement system are assessed experimentally.

## II. METHODOLOGY

### A. MEASUREMENT PRINCIPLE

In this study, a simple marker is placed on the target being measured to enhance the feature of the region of interest on captured images. The marker is fixed on the cross section of a rotor rather than on its cylindrical surface to obtain continuous images during a revolution. Once the rotor is in rotational motion, the speed of the rotor can be measured through detecting the periodic patterns in the captured images. As shown in Fig. 1, a low-cost imaging device is applied to continuously capture the images of the cross section of the rotor. In consideration of the cost-effectiveness and applicability of the measurement system, a common low-cost camera (Logitech USB HD Pro C920 Webcam at a cost of ca US$80) is chosen in this study to assess the performance of the measurement system. The imaging device has a maximum frame rate of 30 fps and supports USB Video Device Class mode. The imaging device offers a range of video formats with different resolutions. In general, images with a higher resolution provide more accurate rotational speed measurement. However, such images result in longer computational time and hence slower system response due to the increasing volume of data to process. In order to strike a balance between the measurement accuracy and the response time of the system, the video is saved in 'I420_160 × 120' format with a total of 19,200 pixels in each image frame.

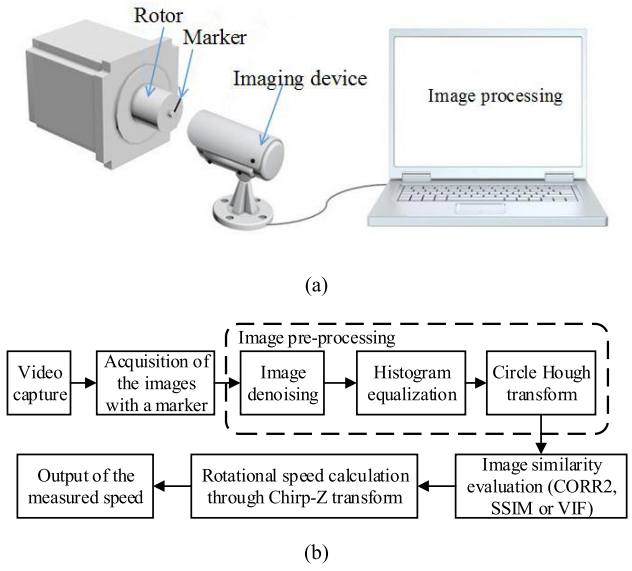


**FIGURE 1.** Imaging based rotational speed measurement system. (a) Sensing arrangement of the measurement system. (b) Principle of the measurement system.

Image similarity evaluation algorithms are used to quantify the similarity between the reference image and the subsequent images. With the continuous processing of the images, the similarity level is regarded as a periodic signal. The periodicity of the similarity level is in fact equal to the time of the rotor rotating for one complete revolution. Chirp-Z transform is deployed to convert the acquired time-domain signal to the frequency domain. The frequency with the highest amplitude in the frequency spectrum of the signal indicating the similarity level is corresponding to the rotational frequency, which is then converted into rotational speed in RPM.

### B. IMAGE PRE-PROCESSING

In order to improve the visual quality of the acquired images and further improve the performance of the measurement system, it is necessary to pre-process the images. Image pre-processing consists of several steps, including image denoising, histogram equalization and circle Hough transform. Since the noise following a zero-mean Gaussian distribution is the most common noise in a real imaging system, a Gaussian filter is used in this study to reduce noise in the images and improve the peak signal-to-noise ratio.

Histogram equalization is used to enhance the image contrast through stretching the pixel values with a dense distribution and merging those in a spare distribution. The histogram equalization process enables the characteristics of the marker on the rotor to be identified easily.

Circle Hough transform is deployed to extract the region of interest with a circular pattern (i.e. the cross section of the rotor) in the image and avoid environmental background interference. Meanwhile, the computational complexity of image similarity evaluation is reduced owing to the fact that only the pixels in the region of interest are processed. The procedures of circle Hough transform include: a set of edge points in the image space are transformed into a Hough parameter space; the parameter space is divided into "buckets" using a grid and an accumulator matrix is produced according to the grid; those edge points on a circle are mapped to the same grid cell, which increases the number of the corresponding matrix element; then the local maxima that indicates the presence of the circular pattern is selected [16]. Fig. 2 illustrates a typical original image and the resulting image after pre-processing.


**FIGURE 2.** The images before and after pre-processing. (a) Original image (b) Preprocessed image.

### C. IMAGE SIMILARITY EVALUATION

Three image processing algorithms, namely, two-dimensional correlation (CORR2), structural similarity (SSIM), and visual information fidelity (VIF) are applied and compared to evaluate image similarity between the reference image and the subsequent ones. In this measurement system, the average of the first 10 images is used as a reference image instead of a single image to avoid the low quality of the reference image and thus ensure the reliability of the measurement. Meanwhile, the reference image, which is determined specially for each test process, can reduce the adverse effect of variations in illumination conditions and help maintain the quality of the similarity levels of acquired images. Through continuous comparison between the reference image and the sequential images, a time-domain signal indicating the similarity level is obtained.

#### 1) TWO-DIMENSIONAL CORRELATION

Two-dimensional correlation (CORR2) is a method for establishing the degree of probability that a linear relationship exists between measured quantities [17]. In this study, the correlation coefficient indicates the degree of similarity between two images with the same size. For two images $X$ and $Y$ with a resolution $m \times n$ pixels, the correlation coefficient $r$ is defined as

$$r = \frac{\sum_{i=1}^{m}\sum_{j=1}^{n}[X(i,j)-\bar{X}][Y(i,j)-\bar{Y}]}{\sqrt{\sum_{i=1}^{m}\sum_{j=1}^{n}[X(i,j)-\bar{X}]^2 \sum_{i=1}^{m}\sum_{j=1}^{n}[Y(i,j)-\bar{Y}]^2}} \quad (1)$$

where $X(i,j)$ and $Y(i,j)$ are the gray-scale values at the point $(i,j)$ in the images $X$ and $Y$, respectively. $\bar{X}$ and $\bar{Y}$ are the mean values of the intensity matrices $X$ and $Y$, respectively. The correlation coefficient has the value $r = 1$ if the two images

are absolutely identical and $r = 0$ if they are completely uncorrelated. As the correlation coefficient is completely invariant to linear transformations of $X$ and $Y$, it offers the robust noise-proof performance and is insensitive to uniform variations in brightness or contrast across an image [18].

#### 2) STRUCTURAL SIMILARITY

SSIM is an image quality metric that assesses the visual impact of three aspects of an image: luminance, contrast and structure. It is used for measuring the similarity between two images and designed to improve traditional methods such as peak signal-to-noise ratio and mean squared error, which are inconsistent with human visual perception [19]. SSIM index is a multiplicative combination of three terms, $l(x, y)$, $c(x, y)$ and $s(x, y)$, which are corresponding to luminance, contrast and structure, respectively, between two image subsets $x$ and $y$. The local SSIM $(x, y)$ is obtained from

$$SSIM(x, y) = l(x, y) \cdot c(x, y) \cdot s(x, y) \tag{2}$$

where

$$l(x, y) = \frac{2\mu_x\mu_y + C_1}{\mu_x^2 + \mu_y^2 + C_1} \tag{3}$$

$$c(x, y) = \frac{2\sigma_x\sigma_y + C_2}{\sigma_x^2 + \sigma_y^2 + C_2} \tag{4}$$

$$s(x, y) = \frac{\sigma_{xy} + C_3}{\sigma_x\sigma_y + C_3} \tag{5}$$

where $\mu_x$, $\mu_y$, $\sigma_x$, $\sigma_y$ and $\sigma_{xy}$ are the local means, standard deviations, and cross-covariance of the two image subsets $x$ and $y$, respectively. $C_1$, $C_2$ and $C_3$ are constants introduced here to avoid zero denominators. These values are somewhat arbitrary, but the performance of the SSIM index algorithm is fairly insensitive to variations of these values. In order to simplify the expression of equation (2), $C_3$ in equation (5) is set to $C_2/2$ [19]. The SSIM index can be described as:

$$SSIM(x, y) = \frac{(2\mu_x\mu_y + C_1)(2\sigma_{xy} + C_2)}{(\mu_x^2 + \mu_y^2 + C_1)(\sigma_x^2 + \sigma_y^2 + C_2)} \tag{6}$$

The mean structural similarity MSSIM of the two images $X$ and $Y$ is defined as

$$MSSIM = \frac{1}{M}\sum_{j=1}^{M} SSIM(x_j, y_j) \tag{7}$$

where $M$ is the number of image subsets in the image and $x_j$ and $y_j$ are the image contents in the $j^{\text{th}}$ image subsets. In this case, the image is segmented into a series of image subsets through a local $11 \times 11$ sliding window, which moves pixel-by-pixel over the entire image. For the image with a resolution of $160 \times 120$, there is a total of 16500 image subsets for MSSIM calculation. The larger MSSIM index, the higher similarity between the two images $X$ and $Y$.

#### 3) VISUAL INFORMATION FIDELITY

The visual information fidelity (VIF) algorithm employs natural scene statistical models in conjunction with a distortion model to quantify the information shared between the reference image and the test image. The more information shared, the higher the similarity. For two $m \times n$ images $X$ and $Y$, VIF index is defined as

$$VIF = \frac{I(X; Y_h)}{I(X; X_h)} \tag{8}$$

where $X_h$ and $Y_h$ indicates the visual signals after the reference image $X$ and the test image $Y$ pass through the human visual system channel, respectively. $I(X; X_h)$ is the information content of the reference image, which is quantified by the mutual information between the input and output of the human visual system channel. $I(X; Y_h)$ denotes the mutual information between the two images $X$ and $Y_h$. In the calculation process, the reference and test images are firstly decomposed into multiple-scale sub-bands through wavelet transform. Then the VIF algorithm measures the visual information by computing mutual information in each sub-band through Gaussian scale mixture modeling, distortion modeling and human visual system modeling, respectively. Finally, the image similarity level is obtained by integrating visual information of all the sub-bands. More details on the VIF are available in [20]. When the rotor is in rotational motion, the VIF index varies with time due to the change of the marker position in the image and thus the fluctuation of the VIF index can reflect the movement of the rotor.

#### 4) ROTATIONAL SPEED CALCULATION

Since the rotor is in rotational motion, the similarity level between the reference image and subsequent images is periodic. The main frequency of the signal indicating the similarity level $f$ is equal to the rotational frequency. Thus the rotational speed $N$ in RPM can be calculated from

$$N = 60f \tag{9}$$

where $f$ is determined through Chirp-Z transform of the signal indicating the similarity level. The peak with the highest amplitude in frequency spectrum is corresponding to the rotational frequency, which is then converted into rotational speed in RPM.

Chirp-Z transform is an effective frequency analysis method which explores the peak response of a signal within a smaller band of frequencies than the total Nyquist frequency spectrum and further refines the low accuracy and resolution of the Fourier spectrum [21]. Given a sequence with a finite length $x(n)$ $(n = 0, 1, \ldots, N-1)$ of the similarity signal, the Chirp-Z transform $X(k)$ of $x(n)$ is defined as

$$X(k) = \sum_{n=0}^{N-1} x(n) Z_M^{kn} (k = 0, 1, \ldots, M-1) \tag{10}$$

where $M$ is the number of sampling points for the Chirp-Z transform with any possible positive integer value. $Z_M^{kn}$ is the

transformation kernel and is determined from

$$Z_M^{kn} = \exp\left\{-j\frac{2\pi n}{f_s}\left[f_0 + \frac{(f_1 - f_0)k}{M}\right]\right\} \tag{11}$$

where $f_s$ is the sampling rate and $[f_0, f_1]$ is the frequency observation interval, which is the priori information about the rough range of the actual rotational frequency. In this study, $f_0$ and $f_1$ are given, respectively, by

$$f_0 = f_F - \frac{f_s}{N}, f_1 = f_F + \frac{f_s}{N} \tag{12}$$

where $f_F$ is coarse frequency estimate, which is calculated as the frequency with the highest amplitude in the frequency spectrum of the signal by applying the Fast Fourier Transform.

Once $X(k)$ is obtained, the power spectrum magnitude of $X(k)$ is given by

$$S(k) = \frac{|X(k)|^2}{n} = \frac{[X_R(k)]^2 + [X_I(k)]^2}{n} \tag{13}$$

where $X_R(k)$ and $X_I(k)$ are the real and imaginary components of $X(k)$, respectively. The maximum value of $S(k)$ at which the Chirp-Z transform converges, on the high-resolution power spectrum, corresponds to the main frequency component of the signal $x(n)$, which is regarded as the fine rotational frequency $f$. The frequency resolution $\Delta f_c$ of the Chirp-Z transform depends on the length of the frequency observation interval and the number of frequency elements covered in the frequency observation interval. $\Delta f_c$ is calculated as

$$\Delta f_c = \frac{f_0 - f_1}{M} \tag{14}$$

According to equations (9) and (14), the resolution of the rotational speed is determined by

$$\Delta N = 60\Delta f_c = \frac{60(f_0 - f_1)}{M} \tag{15}$$

## III. EXPERIMENTAL RESULTS AND DISCUSSION

### A. EXPERIMENTAL SETUP

The measurement system, as shown in Fig. 3, consists of a marker on the cross section of the rotor, the low-cost imaging device to continuously capture images of the rotor, a computer to perform the image processing and rotational speed calculation. The rotor is made of stainless steel with a diameter of 60 mm. The imaging device is placed immediately opposite to the cross section of the rotor, the shooting angle is controlled by a cradle hand and the distance between the rotor and the imaging device is adjustable. A strip-shaped LED light source is used to control the illumination intensity. To create strong color contrast between the rotor and the marker, black markers are used. The acquired images with a resolution of 160 × 120 are transmitted to a host computer via a USB cable for post processing. The host computer includes an Intel(R) Core(TM) i7-4790 3.60 GHz central processing unit, 12 GB computer memory and 2GB video memory and is installed with Microsoft Windows 7 operation system. In order to obtain an independent reference speed to assess the accuracy of the measured speed from the proposed system, a non-contact laser tachometer (UNI-T, model UT372) with a maximum relative error of ±0.04% is used in this study.

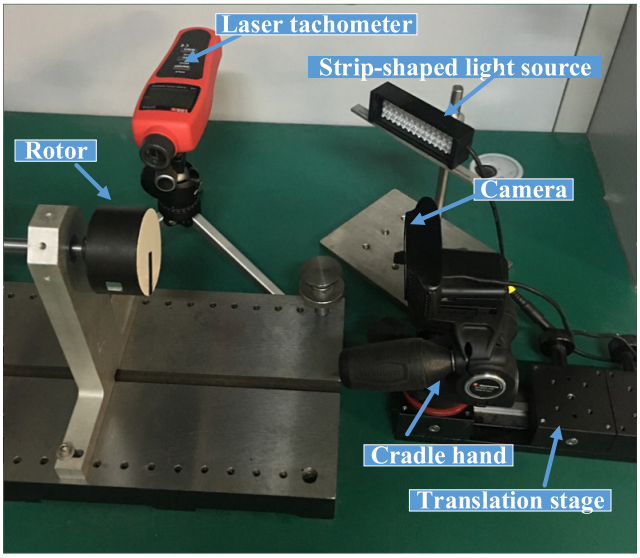


**FIGURE 3.** The integrated rotational speed measurement system.

### B. TEST PROGRAMME

This paper focuses on quantifying the effects of various key factors of the imaging system on the measurement accuracy and reliability of rotational speed and thus identifying the optimal design parameters of the system. The test conditions under which the measurement system was evaluated in this study are summarized in Table 1. Different frame rates (10 fps, 20 fps and 30 fps) of the imaging device are assessed to study its effect on the measurement system (Test I). In order to investigate the effect of marker design on the performance of the measurement system, different shapes and sizes of markers and their positions on the rotor (see Fig. 4) were tested in Tests II & III. The red points in Fig. 4, which do not exist physically in the images, indicate the centre of the rotor. In order to represent and compare the sizes of different markers, the effective area of a marker is normalized to the whole area of the cross-section of the rotor, as outlined in Table 2. The effect of similarity evaluation algorithms on the measurement results is evaluated in Test IV. Test V aims to verify the stability of the system under different illumination conditions. Tests VI and VII are designed to quantify the effects of the shooting angle and photographic distance on the performance of the measurement system, respectively. In this study measurement accuracy is represented in terms of relative error through comparison between the measured speed and the reference speed. The repeatability of the measurement system for a given condition is represented in terms of normalized standard deviation of the measured speed. It should be pointed out that, since the standard deviation data combine both the repeatability of the measurement system and the stability of the motor test rig,

**TABLE 1.** Test programme.

| No | Frame rate (fps) | Marker | | | Similarity evaluation | Illumination (lux) | Angle (°) | Distance (cm) | N (RPM) |
|---|---|---|---|---|---|---|---|---|---|
| | | shape | location | Width or diameter (mm) | | | | | |
| I | 10,20,30 | strip | radial | 8 | CORR2 | 300 | 0 | 20 | 100-900 |
| II | 30 | strip | radial | 8 | CORR2 | 300 | 0 | 20 | 100-900 |
| | | circular | centre | | | | | | |
| | | | edge | | | | | | |
| III | 30 | circular | edge | 2/4/6/8 | CORR2 | 300 | 0 | 20 | 100-900 |
| | | strip | radial | 2/5/8/11 | | | | | |
| IV | 30 | strip | radial | 8 | SSIM/ CORR2/ VIF | 300 | 0 | 20 | 100-900 |
| V | 30 | strip | radial | 8 | CORR2 | 50/300/1000 | 0 | 20 | 100-900 |
| VI | 30 | strip | radial | 8 | CORR2 | 300 | 0/5/ 10/15 | 20 | 100-900 |
| VII | 30 | strip | radial | 8 | CORR2 | 300 | 0 | 5/10/15 /20/25/ 30/35 | 100-900 |

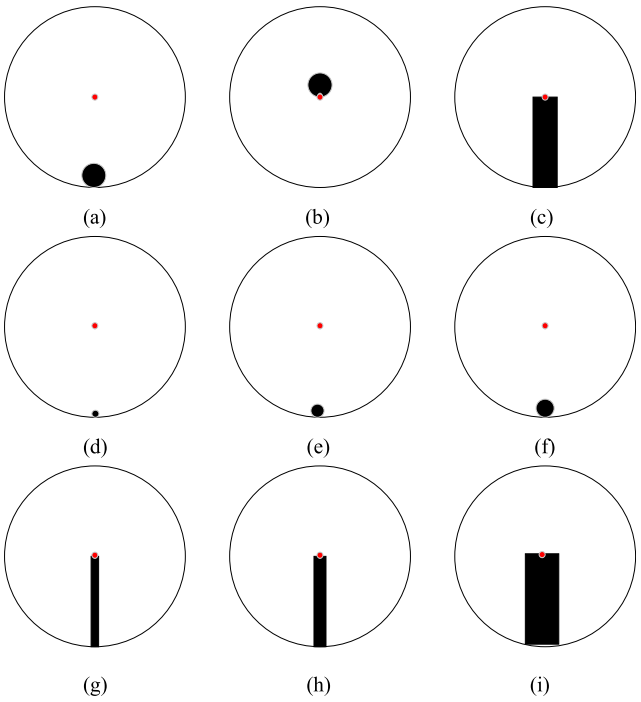


**FIGURE 4.** Different markers for the rotational speed measurement. (a) Circular_8mm_edge. (b) Circular_8mm_centre. (c) Strip-shaped_8mm. (d) Circular_2mm_edge. (e) Circular_4mm_edge. (f) Circular_6mm_edge. (g) Strip-shaped_2mm. (h) Strip-shaped_5mm. (i) Strip-shaped_11mm.

the actual repeatability of the measurement system is better than the normalized standard deviation. A total of 30 measurements under the same test condition were recorded in each repeatability test.

### C. EFFECT OF FRAME RATE

To quantify the effect of the frame rate - an important specification of the measurement system, on the performance of

**TABLE 2.** Marker size with reference to the cross-sectional area of the rotor.

| Marker type | Circular marker | | | | Strip-shaped marker (Marker length = 30mm) | | | |
|---|---|---|---|---|---|---|---|---|
| Marker diameter or width (mm) | 2 | 4 | 6 | 8 | 2 | 5 | 8 | 11 |
| Relative size (%) normalized to the cross-sectional area of the rotor | 0.1 | 0.4 | 1.0 | 1.8 | 2.1 | 5.3 | 8.5 | 11.7 |

the system, a series of experimental tests were conducted with a frame rate of 10 fps, 20 fps and 30 fps, respectively. The CORR2 algorithm was applied for similarity evaluation. Fig. 5 shows that the relative error becomes smaller when the rotational speed increases. When the frame rate is 30 fps, the relative error at the speed of 100 RPM are around $-0.6\%$ with the normalized standard deviation of about 0.5%, while the error is significantly reduced to within $\pm 0.1\%$ when the rotational speed increases. This outcome is due to the fact that more rotating periods are available for spectral analysis at a higher speed during the same sampling time. It is evident that the measured rotational speed at 200 RPM or lower is consistently smaller than the reference speed. It is thought to be due to the fact that the reference tachometer is based on the principle of pulse counting. An incomplete circular motion is frequently regarded as a complete revolution and hence overestimation of the rotational speed whereas the proposed method has no this problem. The measurement error of the reference tachometer under very low rotational speeds may be greater than the measurement accuracy stated in its operation manual. When the rotor rotates at a lower speed, the spectrum refinement algorithm, Chirp-Z transform, has little effect on compensation of accuracy due to less rotating period for spectral analysis, which results in a higher error of measurement result. It is also noticeable that the normalized standard

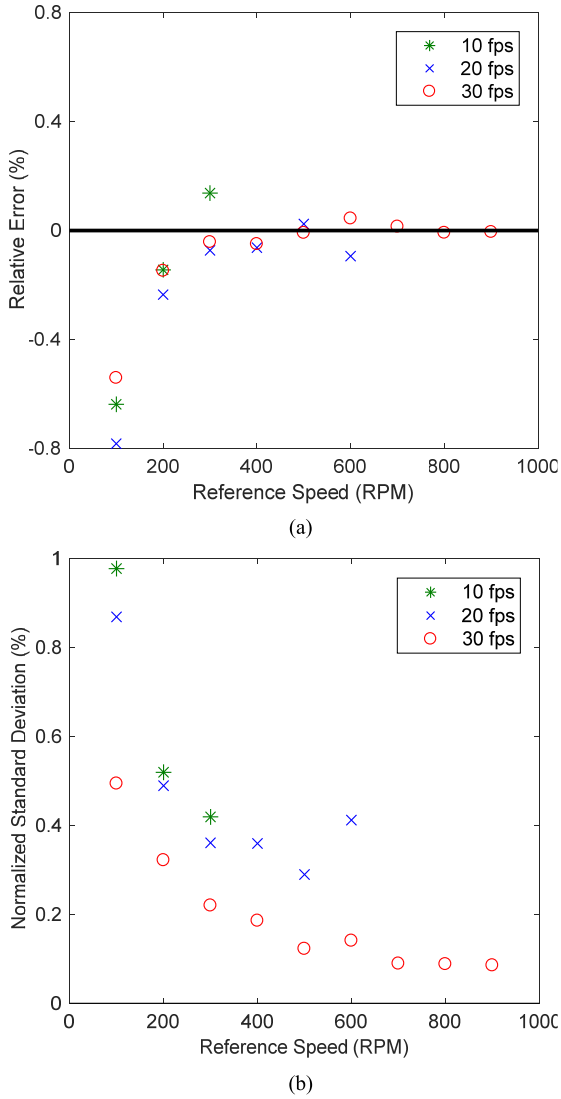


**FIGURE 5.** Test results for different frame rates. (a) Relative error. (b) Normalized standard deviation.

deviation decreases with the rotational speed and thus the stability of the system is enhanced. As expected, there exists motion blur in the images when the rotational speed increases. The motion blur can be alleviated, to some extent, through adjusting the exposure time at a lowest-as-possible value. In this paper, the rotational speed measurement is achieved through frequency analysis, i.e. determining the periodicity of the image similarity signal. Motion blur has a similar impact on sequential images when the rotor rotates at a constant speed and thus there is little effect on the periodicity of the image similarity signal. The proposed measurement strategy makes the proposed system little affected by motion blur. As expected, a higher frame rate provides more accurate and stable results due to smoother similarity level signals with more sampling points.

Additionally, the 'missing' data points for 10 fps and 20 fps in Fig. 5 are due to the fact that the frame rate limits the measurement range of the rotational speed because of temporal aliasing. According to the Nyquist sampling criterion, the frame rate of the camera must be at least twice of the rotational frequency. In this case, the maximum measurable speed for a given frame rate ($f_s$) is ($30\times f_s$) RPM.

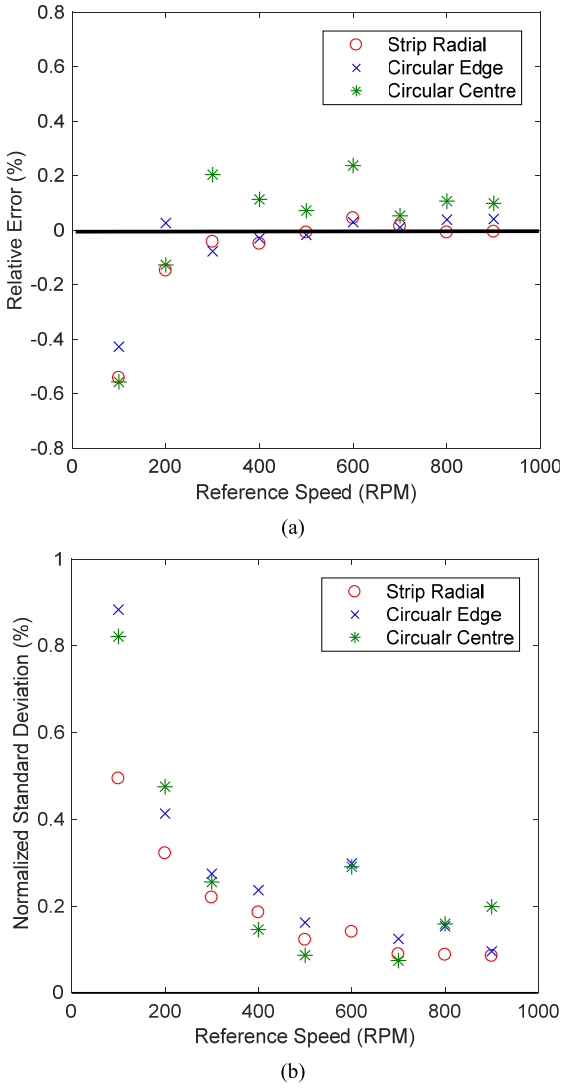


**FIGURE 6.** Test results for different marker positions. (a) Relative error. (b) Normalized standard deviation.

### D. EFFECT OF MARKER DESIGN

Experimental tests were conducted to study the effect of maker size, shape and position on the system performance in terms of accuracy and repeatability. Marker design is an important factor for the proposed system. The marker color is not a critical issue as long as the marker can be easily recognized from the image background. Fig. 6 depicts the results for the circular markers placed on the edge and close to the center of the rotor and a strip-shaped marker along the radial direction of the cross section. The circular makers have a diameter of 8 mm whilst the strip-shaped maker has a dimension of 8 mm $\times$ 30 mm.

As shown in Fig. 6, the circular marker placed on the edge of the rotor generates more accurate and repeatable results than that close to the rotor centre. Since the marker on the edge travels over a longer angular distance for the same time interval, the difference in the similarity levels is evident. In comparison with the circular marker, the strip-shaped marker with the same width has a better repeatability as it behaves like an array of multiple markers along the same radius and hence more information is derived from the images.

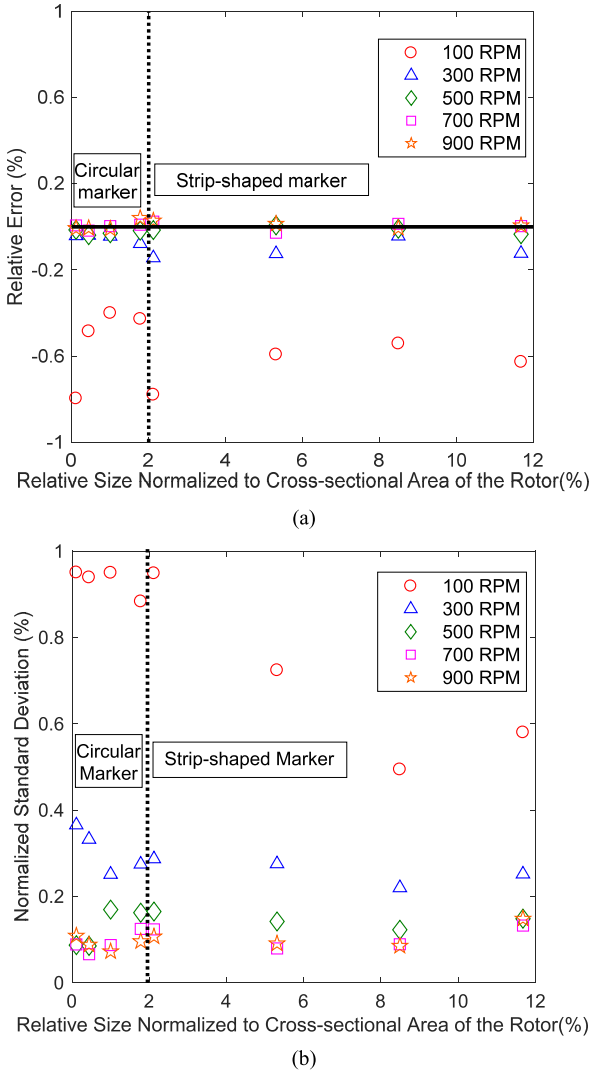


**FIGURE 7.** Test results for different markers. (a) Relative error. (b) Normalized standard deviation.

To further explore the effect of the marker size on the system performance, strip-shaped markers with different widths (2 mm, 5 mm, 8 mm and 11 mm) of the same length and circular makers placed on the edge of the rotor with a diameter of 2 mm, 4 mm, 6 mm, and 8 mm were tested, respectively. Results shown in Fig. 7 suggest that rotational speed can be measured accurately even the marker is as small as 0.1% of the cross sectional area of the rotor. Besides, the marker with a width of 8 mm outperforms other makers in terms of accuracy and repeatability. An explanation for this result is that a small sized marker has little influence on the grayscale distribution of captured images, and thus the accuracy and repeatability of the measurement system are reduced. In contrast, large deformation of the marker edge may be introduced due to motion blur. If the marker size is exceedingly large, the grayscale distribution of the marker in the image will be changed.

**TABLE 3.** Comparison of the mean processing time (in ms) of similarity evaluation algorithms.

| Similarity evaluation algorithm | CORR2 | SSIM | VIF |
|---|---|---|---|
| Mean processing time | 0.28 | 3.5 | 47 |

### *E. COMPARISON OF DIFFERENT SIMILARITY EVALUATION ALGORITHMS (CORR2, SSIM, AND VIF)*

Fig. 8 shows the typical image similarity signals obtained under the same test conditions using CORR2, SSIM and VIF algorithms, respectively. The reference speed was set to 100 RPM and the frame rate of the camera was 30 fps. We can see that the three image similarity evaluation algorithms yield a similar periodicity but different similarity levels. CORR2 generates the highest similarity index as CORR2 only quantifies the pixel intensity of the image. In addition, the computational complexity of the three image similarity evaluation algorithms is very different. Table 3 outlines the mean processing time of one thousand images using the algorithms, respectively. It can be seen that CORR2 has the lowest computational complexity than the other two algorithms. Results in Fig. 9 indicate that CORR2 and SSIM have given similar relative errors but smaller normalized standard deviation than VIF for the same speed. The reason for this difference is that VIF considers more effects of environmental factors on the visual impact of images when computing image similarity, while the SSIM and CORR2 are insensitive to uniform variations in brightness or contrast across an image. It is worth noting that CORR2 is more efficient than SSIM and VIF and thus CORR2 algorithm is used to obtain the image similarity evaluation in the following study.

### *F. EFFECT OF ILLUMINATION CONDITIONS*

In practical applications the illumination conditions can vary significantly, which may affect the performance of an imaging based measurement system. To observe this effect, experimental tests were conducted under three different illumination conditions: weak, normal and strong light sources. A strip-shaped light source with adjustable light intensity was used to generate weak light (50 lux), normal light (300 lux) and strong light (1000 lux), respectively. As shown in Fig. 10, the relative error is very similar and

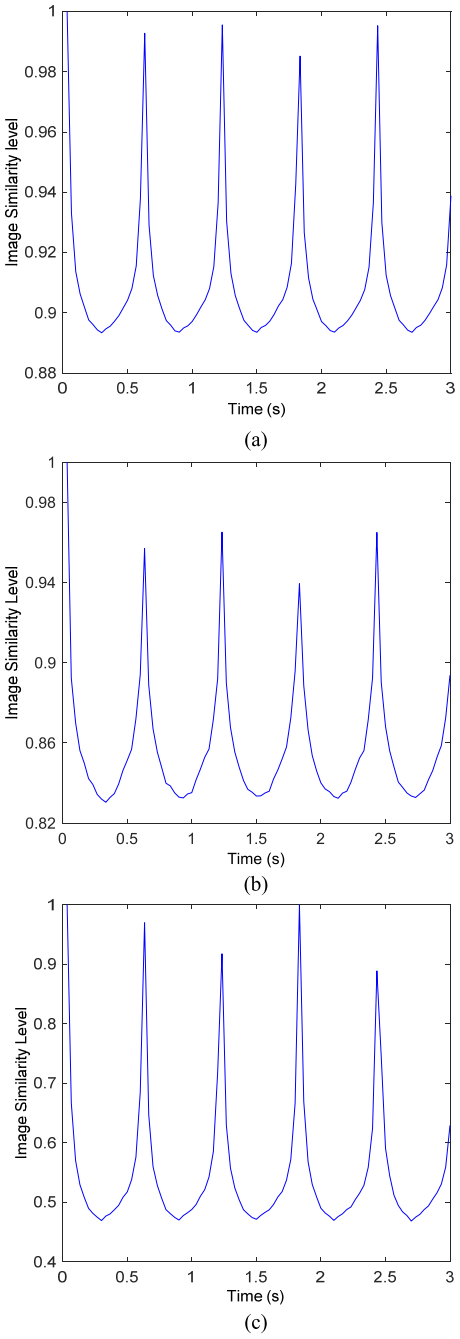


**FIGURE 8.** Time domain results for image similarity evaluation. (a) CORR2. (b) SSIM. (c) VIF.

standard deviation is less than 0.5% under different light intensities, which indicates the measurement system is robust enough even under weak or strong illumination conditions. However, weak or strong illumination has little effect on the repeatability of the system. The normalized standard deviation with weak and strong illumination conditions is slightly larger than that with normal light. This is due to the poor contrast between the rotor and the marker under the weak and strong light conditions, which may result in uncertainty in image similarity evaluation.

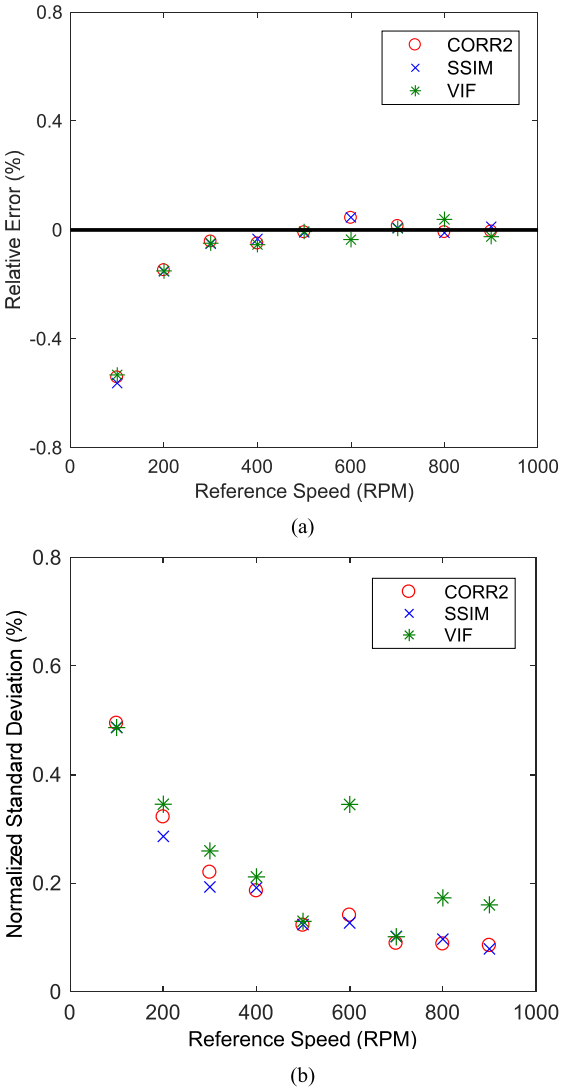


**FIGURE 9.** Test results for different image similarity evaluation algorithms. (a) Relative error. (b) Normalized standard deviation.

### G. EFFECT OF SHOOTING ANGLE

The shooting angle of the imaging device may not be ideal in practical applications of the system. Experimental assessments were thus conducted for four different shooting angles: 0°, 5°, 10° and 15°. The different shooting angles are implemented with a cradle head which can change the shooting angle between the optical axis of the camera and the cross section of the rotor. As shown in Fig. 11, both the relative error and normalized standard deviation increase with the shooting angle, which is attributed to image distortion and object occlusion caused by the change of the view field of the camera. As expected, the system has a better performance when the optical axis of the imaging device is vertical to the cross section of area because of the smallest distortion of the camera. It is also noticeable that the measurement accuracy is still satisfactory and standard deviation is less than 1% even when the shooting angle is 15°, which demonstrates the measurement system is robust enough for a range of shooting angles.

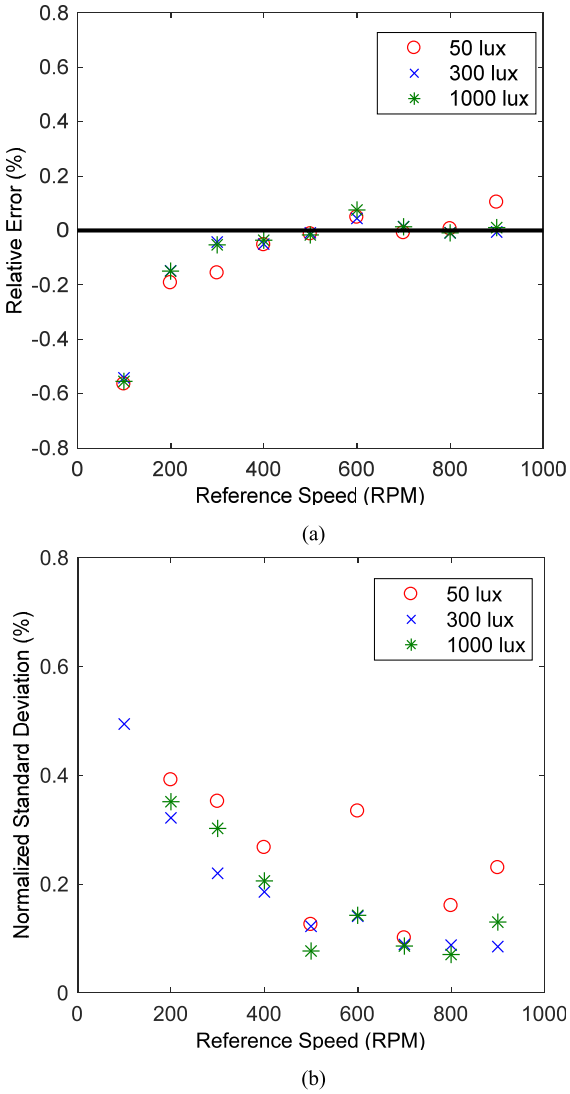


**FIGURE 10.** Test results under different illumination conditions. (a) Relative error. (b) Normalized standard deviation.

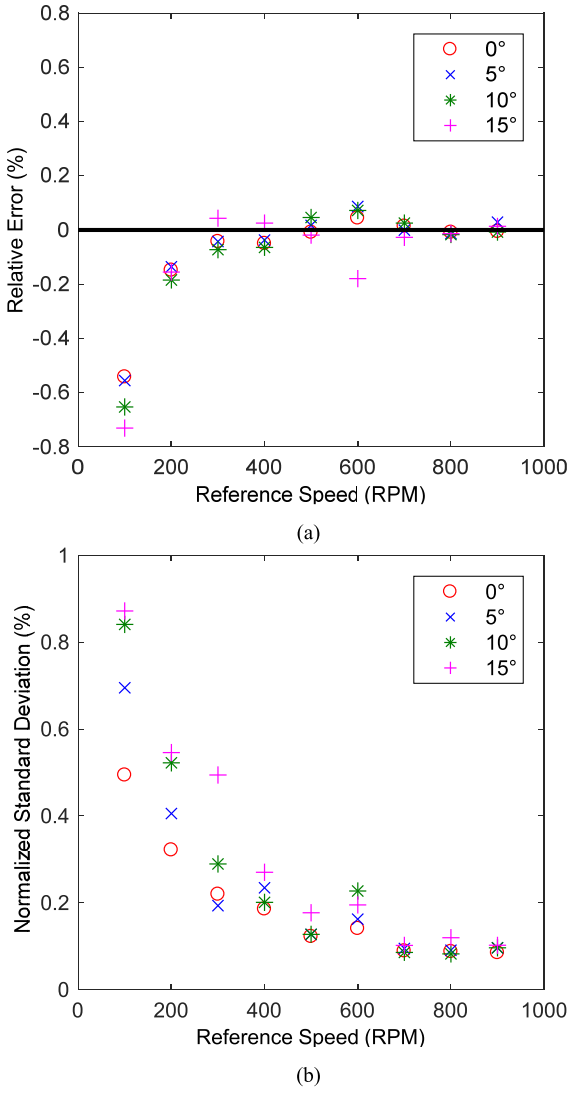


**FIGURE 11.** Test results for different shooting angles. (a) Relative error. (b) Normalized standard deviation.

### *H. EFFECT OF PHOTOGRAPHIC DISTANCE*

In order to determine the best distance between the imaging device and the rotor, experimental tests were conducted for different photographic distances. The camera was mounted on a translation stage, allowing the photographic distance to be adjusted from 5 cm to 35 cm. The results shown in Fig. 12 demonstrate that the measurement system performs the best at the photographic distance of 20 cm. Under this circumstance, the image content covers the whole cross section of the rotor, enabling high image similarity and enhanced periodicity of the signal. In general, a longer photographic distance will reduce the spatial resolution of images, leading to a smaller rotor image on the imaging plane and thus reducing the effect of the marker on the gray distribution of the image. In contrast, once the distance between the rotor and the imaging device is shorter than 20 cm, the rotor area cannot be fully covered by the acquired image due to the limitation of the view field of the imaging device. In this case the correlation coefficient between the captured images is reduced and the performance of the measurement system degraded. Under very low speeds such as 100 RPM the system gives large errors with poor repeatability over the whole range of the shooting distance. This result is consistent with the observations in Section III.C.

### *I. DYNAMIC MEASUREMENT OF VARYING ROTATIONAL SPEED*

The effectiveness of the imaging system for dynamic measurement of time-varying rotational speed is also verified. The rotational speed is manually adjusted by varying the voltage applied to the servo motor. For the imaging device with a frame rate of 30 fps, 30 images with a sampling period of one second are acquired for each measurement. In this case, the measured rotational speed is the mean speed during the sampling period. In general, more images for each measurement of rotational speed entail a higher measurement

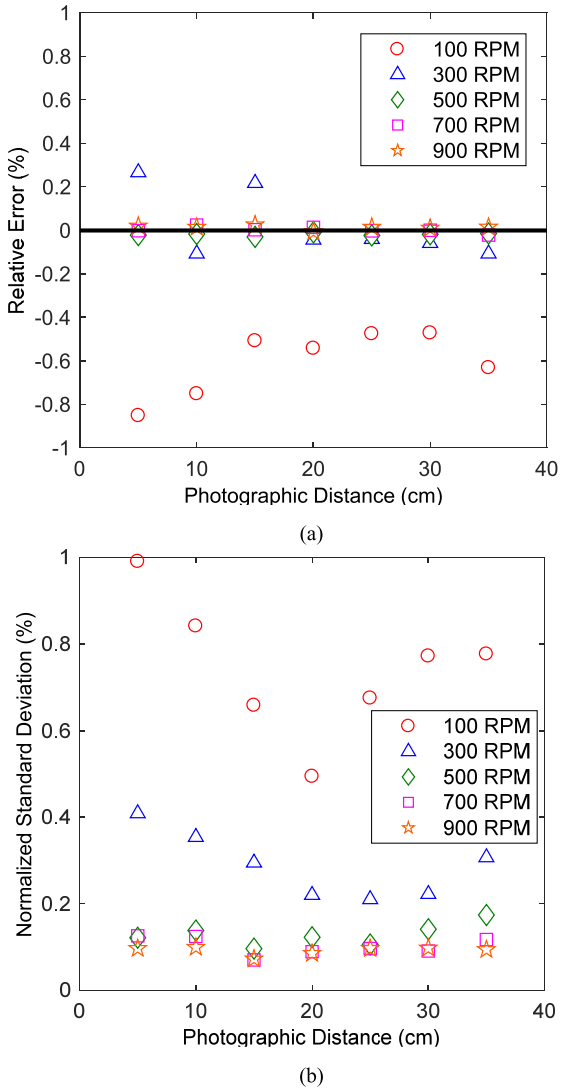


**FIGURE 12.** Test results for different photographic distances. (a) Relative error. (b) Normalized standard deviation.

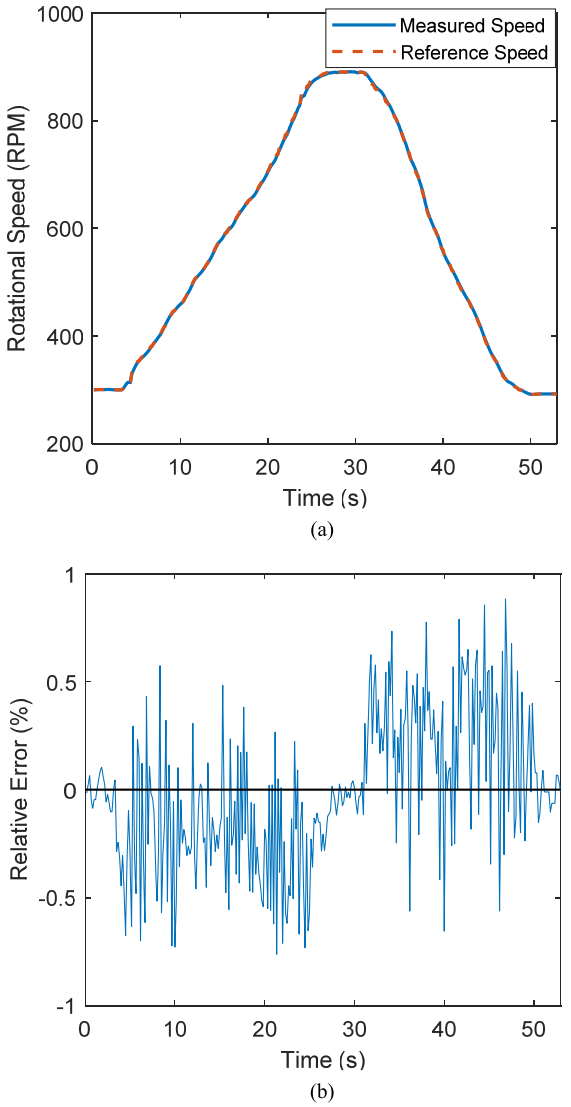


**FIGURE 13.** Test results for dynamic measurement of rotational speed. (a) Measured speed versus the reference speed. (b) Relative error .

accuracy but at the expenses of higher computation complexity and hence longer repsonse time. In the measurement process, each newly acquired image together with the previous 29 images is used for rotational speed calculation. This means that the proposed system is capable of providing 30 rotational speed measurements per second. In this experiment the whole data recording time is 53 s. As shown in Fig. 13, the reference speed and the measured speed are in agreement with each other, which demonstrates that the imaging system can provide instantaneous rotational speed measurement with a relative error within $\pm 1\%$ under non-stationary operating conditions. As expected, the measurement error under dynamic conditions is larger than that under steady speed conditions due to the non-stationary nature of the similarity level signal.

It should be noted that the mean speed during the time interval of $[t - 0.5, t + 0.5]$ indicates the rotational speed at the time of $t$. After the images are acquired, the total calculation time of each measurement $T_e$, including image preprocessing, image similarity evaulation, and spectral analysis, is approximately 0.057 second. Therefore, the measurement response delay is approximately $(0.5 + T_e)$ second, namely 0.557 s. In other words, the rotational speed at the time of $t$ is determined at the time of $(t + 0.557)$, which can meet the requirements of real-time condition monitoring and control of mechanical systems.

## IV. CONCLUSIONS

Experimental results under different test conditions suggest that the low-cost imaging device based rotational speed measurement system performs very well in terms of accuracy and repeatability. When the strip marker with a width of 8 mm is applied, the measurement system with a frame rate of 30 fps is capable of providing constant rotational speed measurements with a relative error of no greater than $\pm 0.6\%$ with the maximum normalized standard deviation of 0.6% over the

speed range from 100 to 900 RPM. For rotational speeds over 300 RPM, both the measurement error and the normalized standard deviation are consistently within ±0.1%. Meanwhile, the system can measure time-varying rotation speed with a relative error within ±1%. The results presented have indicated that two-dimensional correlation is a more suitable algorithm than SSIM and VIF in terms of accuracy and repeatability. It is evident that illumination conditions have little effect on the measurement results and the measurement system is robust even though the optical axis of the imaging device is not aligning significantly to the rotor center. Additionally, the measurement system yields the better performance when the photographic distance is 20 cm. In this case, the captured images cover the whole rotor area with less background information. In order to further improve the cost-effectiveness and portability of the imaging method for rotational speed measurement, a highly integrated system capable of capturing image data and translating the data into meaningful measurements through embedded computing, such as a Raspberry Pi or a mobile phone, will be developed in the future.

## REFERENCES

[1] S. D. Yu and X. Zhang, "A data processing method for determining instantaneous angular speed and acceleration of crankshaft in an aircraft engine–propeller system using a magnetic encoder," *Mech. Syst. Signal Process.*, vol. 24, no. 4, pp. 1032–1048, 2010.

[2] Y. S. Didosyan, H. Hauser, H. Wolfmayr, J. Nicolics, and P. Fulmek, "Magneto-optical rotational speed sensor," *Sens. Actuators A, Phys.*, vol. 106, nos. 1–3, pp. 168–171, 2003.

[3] Y. Li, F. Gu, G. Harris, A. Ball, N. Bennett, and K. Travis, "The measurement of instantaneous angular speed," *Mech. Syst. Signal Process.*, vol. 19, no. 4, pp. 786–805, 2005.

[4] R. Myers, R. A. Islam, M. Karmarkar, and S. Priya, "Magnetoelectric laminate composite based tachometer for harsh environment applications," *Appl. Phys. Lett.*, vol. 91, no. 12, pp. 122904-1–122904-3, 2007.

[5] L. Wang, Y. Yan, Y. Hu, and X. Qian, "Rotational speed measurement through electrostatic sensing and correlation signal processing," *IEEE Trans. Instrum. Meas.*, vol. 63, no. 5, pp. 1190–1199, May 2014.

[6] L. Wang, Y. Yan, Y. Hu, and X. Qian, "Rotational speed measurement using single and dual electrostatic sensors," *IEEE Sensors J.*, vol. 15, no. 3, pp. 1784–1793, Mar. 2015.

[7] J. Urbanek, T. Barszcz, and J. Antoni, "A two-step procedure for estimation of instantaneous rotational speed with large fluctuations," *Mech. Syst. Signal Process.*, vol. 38, no. 1, pp. 96–102, 2013.

[8] H. Lin and K. Ding, "A new method for measuring engine rotational speed based on the vibration and discrete spectrum correction technique," *Measurement*, vol. 46, no. 7, pp. 2056–2064, 2013.

[9] D. Luvizon, B. Nassu, and R. Minetto, "A video-based system for vehicle speed measurement in urban roadways," *IEEE Trans. Intell. Transp. Syst.*, vol. 18, no. 6, pp. 1393–1404, Jun. 2017.

[10] J. Guo, C. Zhu, S. Lu, D. Zhang, and C. Zhang, "Vision-based measurement for rotational speed by improving Lucas–Kanade template tracking algorithm," *Appl. Opt.*, vol. 55, no. 25, pp. 7186–7194, 2016.

[11] J. Zhong, S. Zhong, Q. Zhang, and Z. Peng, "Measurement of instantaneous rotational speed using double-sine-varying-density fringe pattern," *Mech. Syst. Signal Process.*, vol. 103, no. 3, pp. 117–130, Mar. 2018.

[12] X.-D. Zhu and S.-N. Yu, "Measurement angular velocity based on video technology," in *Proc. Int. Congr. Image Signal Process. (CISP)*, Shanghai, China, Oct. 2011, pp. 1936–1940.

[13] X. Zhang, J. Chen, Z. Wang, N. Zhan, and R. Wang, "Digital image correlation using ring template and quadrilateral element for large rotation measurement," *Opt. Laser Eng.*, vol. 50, no. 7, pp. 922–928, 2012.

[14] L. Wang, Y. Yan, Y. Hu, and X. Qian, "Radial vibration measurement of rotary shafts through electrostatic sensing and Hilbert–Huang transform," in *Proc. IEEE Int. Instrum. Meas. Technol. Conf.*, Taipei, Taiwan, May 2016, pp. 867–871.

[15] Y. Wang, L. Wang, and Y. Yan, "Rotational speed measurement through digital imaging and image processing," in *Proc. IEEE Int. Instrum. Meas. Technol. Conf.*, Turin, Italy, May 2017, pp. 260–265.

[16] T. J. Atherton and D. J. Kerbyson, "Size invariant circle detection," *Image Vis. Comput.*, vol. 17, no. 11, pp. 795–803, 1999.

[17] A. Kaur, L. Kaur, and S. Gupta, "Image recognition using coefficient of correlation and structural similarity index in uncontrolled environment," *Int. J. Comput. Appl.*, vol. 59, no. 5, pp. 32–39, Dec. 2012.

[18] B. Pan, K. Qian, H. Xie, and A. Asundi, "Two-dimensional digital image correlation for in-plane displacement and strain measurement: A review," *Meas. Sci. Technol.*, vol. 20, no. 6, p. 062001, 2009.

[19] Z. Wang, A. C. Bovik, H. R. Sheikh, and E. P. Simoncelli, "Image quality assessment: From error visibility to structural similarity," *IEEE Trans. Image Process.*, vol. 13, no. 4, pp. 600–612, Apr. 2004.

[20] H. R. Sheikh and A. C. Bovik, "Image information and visual quality," *IEEE Trans. Image Process.*, vol. 15, no. 2, pp. 430–444, Feb. 2006.

[21] D. Granados-Lieberman, R. J. Romero-Troncoso, E. Cabal-Yepez, R. A. Osornio-Rios, and L. A. Franco-Gasca, "A real-time smart sensor for high-resolution frequency estimation in power systems," *Sensors*, vol. 9, no. 9, pp. 7412–7429, 2009.

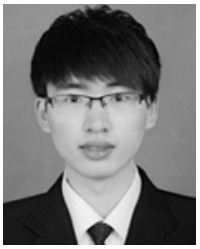

**TIANYU WANG** (M'18) received the B.Eng. degree in information and computing science and the M.Sc. degree in control engineering from North China Electric Power University, Beijing, China, in 2013 and 2016, respectively, where he is currently pursuing the Ph.D. degree in measurement and automation. His current research interests include digital image processing, computer vision, and condition monitoring of mechanical systems.

**YONG YAN** (M'04–SM'04–F'11) received the B.Eng. and M.Sc. degrees in instrumentation and control engineering from Tsinghua University, Beijing, China, in 1985 and 1988, respectively, and the Ph.D. degree in flow measurement and instrumentation from the University of Teesside, Middlesbrough, U.K., in 1992.

He was an Assistant Lecturer with Tsinghua University in 1988. He joined the University of Teesside, as a Research Assistant, in 1989. He was a Lecturer with the University of Teesside from 1993 to 1996, and then a Senior Lecturer, Reader, and Professor with the University of Greenwich, Chatham, U.K., from 1996 to 2004. He is currently a Professor of electronic instrumentation, the Head of the Instrumentation, Control and Embedded Systems Research Group, and the Director of Research with the School of Engineering and Digital Arts, University of Kent, Canterbury, U.K. He has been an Adjunct Professor with North China Electric Power University, Beijing, China, since 2011. He has published over 400 research papers in journals and conference proceedings with an h-index of 40. His current research interests include multiphase flow measurement, combustion instrumentation, and intelligent measurement and condition monitoring.

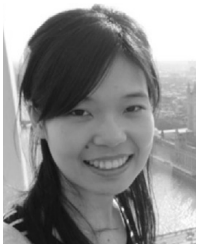

**LIJUAN WANG** (M'18) received the B.Eng. degree in computer science and technology from Qiqihar University, Heilongjiang, China, in 2010, and the Ph.D. degree in measurement and automation from North China Electric Power University, Beijing, China, in 2015, and the Ph.D. degree in electronic engineering from the University of Kent, Canterbury, U.K., in 2017. She is currently a Lecturer in electronic instrumentation with the School of Engineering and Digital Arts, University of Kent. Her current research interests include electrostatic sensing, multiphase flow measurement, intelligent instrumentation, and condition monitoring.

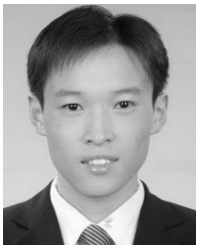

**YONGHUI HU** (M'11) received the B.Eng. degree in automation from the Beijing Institute of Technology, Beijing, and the Ph.D. degree in dynamics and control from Peking University, Beijing, in 2004 and 2009, respectively.

He was a Post-Doctoral Research Fellow with Beihang University, Beijing, from 2010 to 2012. He is currently an Associate Professor with the School of Control and Computer Engineering, North China Electric Power University, Beijing. His current research interests include measurement of multiphase flow and condition monitoring of mechanical systems.